DOI: 10.61782/fa.2025.0419

FORUM ACUSTICUM EURONOISE 2025

FURTHER INVESTIGATION OF THE SIMPLIFIED SEPTA ACOUSTIC LINER CONCEPT

Brian M. Howerton[1*] **Jordan R. Kreitzman**[1]
[1] Applied Acoustics Branch, NASA Langley Research Center, USA

ABSTRACT

Additional refinements of an acoustic liner design incorporating single-hole perforate septa were evaluated by the NASA Langley Liner Physics Team. The design, termed the 'Simplified Septa' concept, incorporates embedded septa as found in traditional, multidegree-of-freedom liners. Typically, such septa are either multihole perforates or porous mesh, whereas the Simplified Septa uses only one hole per cell. An optimization scheme was employed to determine the liner geometry based on a target absorption cost function. These optimized designs incorporating one and two septa were tested in the NASA Langley Normal Incidence Tube (NIT) to determine impedance and absorption spectra for swept tonal excitation at 120 and 140 dB. Experimental results were compared to predictions from a liner model based on the Zwikker-Kosten Transmission Line (ZKTL) code and showed good agreement for no-flow conditions. Absorption performance was found to be good over a wide portion of the frequency range tested. The single-septum design geometry was applied to a larger sample suitable for evaluation in the NASA Langley Grazing Flow Impedance Tube (GFIT). The sample was subjected to grazing flow speeds up to Mach 0.5 and swept tonal excitation at 120 and 140 dB to determine its impedance under these conditions. The results gave confidence that the concept could be used successfully in a grazing flow environment.

Keywords: *acoustic liner, impedance, septa, normal incidence, optimization*

1. INTRODUCTION

Certification requirements limit the noise levels commercial aircraft can produce during operations. Aircraft engines are typically the primary contributor to the overall noise spectrum with the engine fan being a significant contributor [1]. The application of acoustic liners to the walls of the inlet and aft bypass ducts of turbofan engines has been highly effective in reducing total engine noise [2–4]. Engine design trends have led to reduced tonal levels relative to the broadband components of the total noise spectrum [5]. Thus, liner concepts with wider absorption bandwidth are of interest for future applications.

Examples of liners typically used in aircraft engines are shown in Figure 1. Single-degree-of-freedom (SDOF) liners provide excellent absorption for a narrow range of frequencies (approximately one octave) controlled through the choice of cavity depth and facesheet geometry. Widening this frequency range can be achieved by embedding a porous septum within the liner core to create a two-degree-of-freedom (2DOF) liner. The additional resonant frequencies extend the effective absorption range to two octaves. Using additional septa can widen this further but with additional complexity and cost.

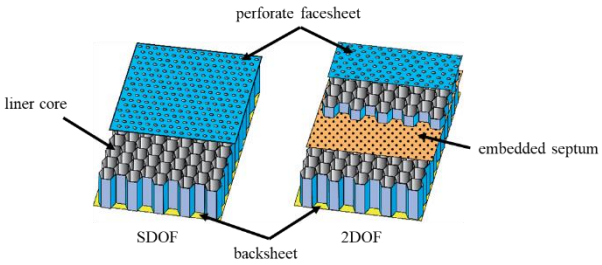

Figure 1. Conventional liner construction.

[*] ***Corresponding author***: *brian.m.howerton@nasa.gov*

A previous paper detailed the development of the Simplified Septa (SS) liner concept whereby embedded septa employing a single perforation were used. Results showed good broadband performance for optimized 2- and 3-septa configurations [6]. The current work continues the development of the concept through testing a new set of 1- and 2-septa designs optimized for absorption from 600-3000 Hz at 140 dB tonal excitation. Samples were manufactured using stereolithography and evaluated in the NASA Langley Normal Incidence Tube (NIT) at source sound pressure levels (SPLs) of 120 and 140 dB to determine their acoustic performance. One configuration was also evaluated using the NASA Langley Grazing Flow Impedance Tube (GFIT) for the same frequencies and SPLs at Mach numbers up to 0.5 to determine if the concept performs adequately when exposed to flow.

2. BACKGROUND

2.1 Simplified Septa Concept

The SS concept is an alternative embodiment of the typical 2DOF liner that may be attractive for certain applications. The use of a single-hole septum perforate can simplify manufacturing of the liner core. The required perforations could be punched, drilled or lasered (depending on diameter) either before or after septum placement. Additive manufacturing (AM) could be readily applied as the perforations are large enough to be within the limits of such methods. The use of a single hole generates dissipation through the creation of vortical structures separating from the hole edges, especially at high SPLs. The resultant liner is, therefore, nonlinear with increasing acoustic levels.

2.2 Septa Optimization

Determination of the liner facesheet properties along with septa placement, hole diameter and liner depth were done via an optimization process. The liner was modeled using a version of the NASA Zwikker and Kosten Transmission Line (ZKTL) impedance prediction code [7–10]. The impedance modeling approach was implemented in a set of Python scripts and coupled with a nonlinear optimization routine, NLopt [11]. Specifically, the BOBYQA [12] algorithm was implemented, which is a derivative free bound constrained local minimum solver.

Constraints were imposed upon the various geometric parameters of the liner as shown in Table 1. The bounds were chosen to ensure resulting designs could be manufactured with available methods but provides latitude for parameter values outside of those found in production liners. Note that septa placement was done as a percentage of the available height and bounded to prevent placement either too close to the facesheet, backplate or other septa. Figure 2 provides a diagram of a liner unit cell with pertinent dimension labels. Note that the number of septa used was a fixed parameter, not a variable in the optimization.

Table 1. Simplified Septa liner optimization constraints.

	Description	Lower Bound	Upper Bound
Facesheet	hole dia. (d_n)	0.51 mm	1.52 mm
	thickness (t_n)	0.51 mm	2.54 mm
	POA	4 %	16 %
Septa	hole dia. (d_n)	0.51 mm	3.81 mm
	thickness (t_n)	0.51 mm	1.52 mm
Cavities	total length (L)	7.62 mm	43.18 mm
	L_n (% of available height)	10	90

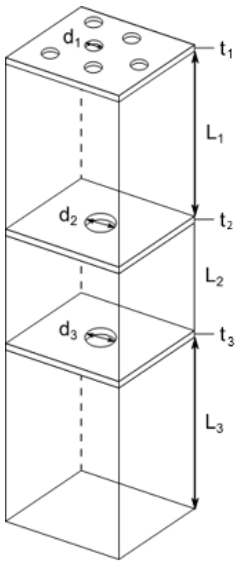

Figure 2. AM liner core unit cell diagram.

An objective function based on maximizing the computed absorption coefficient over a desired frequency range was used. If X is a vector of the liner design variables, then the

average absorption coefficient over a given frequency range can be expressed as:

$$\bar{\alpha} = \frac{1}{f_2 - f_1}\int_{f_1}^{f_2} \alpha(X)df \quad (1)$$

where f_1 and f_2 are the lowest and highest frequencies of interest. For the current study, these frequencies were set to 600 and 3000 Hz to reflect the majority of the testing range. A source SPL of 140dB was chosen for the optimization to more closely match the expected SPLs of a practical engine application.

3. EXPERIMENT

Liner samples were constructed using AM and consist of the liner core and a separable facesheet fabricated via a stereolithography process whereby liquid plastic resin is photopolymerized to build the part. The experimental investigation involves two phases of testing. The first evaluated two configurations in the NASA Langley NIT to determine their impedance and absorption spectra. These results were used to downselect a configuration for Phase 2 testing in the grazing flow environment of the GFIT test rig.

3.1 Liner Core Construction

The AM liners for the NIT testing employed a 5x5 grid of 7.62 mm square unit cells separated by 2.54 mm partitions forming a total sample area of 2581 mm^2. This sample area matches the cross-section area of the NIT waveguide. Table 2 lists dimensions for the two Phase 1 core samples, the first with one embedded septum per cell (AM1S) and the second with two embedded septa per cell (AM2S). Images of the core samples are provided in Fig. 3 showing the embedded septa in each cell.

Table 2. Liner core unit cell dimensions.

Dimension (mm)	1 Septa (AM1S)	2 Septa (AM2S)
t_1	1.32	1.35
d_1	0.56	0.99
L_1	26.49	24.08
t_2	0.30	0.30
d_2	1.19	1.42
L_2	16.76	12.19
t_3	N/A	0.30
d_3	N/A	0.79
L_3	N/A	7.7
Total Length	29.85	

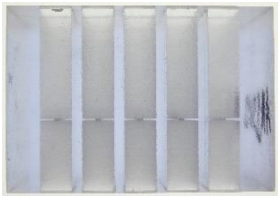

a) AM1S

b) AM2S

Figure 3. Side view of AM liner core samples.

An additional core sample, based on the AM1S unit cell geometry, was constructed for Phase 2 testing in the GFIT. The sample was an extended replication of the NIT liner geometry, creating a 5x40 cell grid with dimensions of 50.8 x 254 mm (width x length).

3.2 Liner Facesheet Construction

Each core was paired with a printed facesheet with unique porosity, hole geometry, spacing and thickness. The AM1S sheet (Fig. 4a) is 1.32 mm thick and has a percent open area (POA) of 13.3 using 28 0.56 mm diameter circular holes per cell distributed in a staggered pattern. The facesheet for AM2S (Fig. 4b) is 1.35 mm thick with a POA of 11.8 and ten 0.99 mm diameter holes per cell (again in a uniform, staggered pattern). The facesheet for the GFIT sample is based on the AM1S geometry from Table 2, but rather than being a separate part, was integrally constructed with the core.

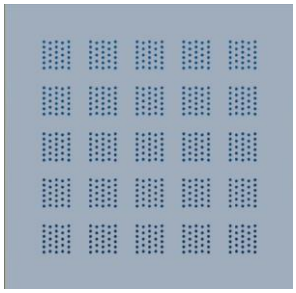

a) AM1S

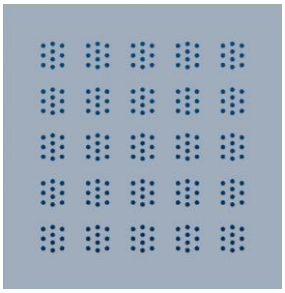

b) AM2S

Figure 4. Top view of AM liner facesheets.

3.3 Experimental Test Rigs

3.3.1 Normal Incidence Tube (Phase 1)

The NIT consists of a group of six electromagnetic acoustic drivers coupled radially into a cylindrical tube that transitions to the 50.8 mm x 50.8 mm square cross-section waveguide. Samples are placed at the exit of the tube to be exposed to the generated sound field. Individual digital-to-

analog converters for each speaker allow for the creation of arbitrary waveforms to energize each driver. Typically, tonal or broadband signals are employed for impedance eduction. Impedance spectra for each sample are obtained in the NIT via the switching Two-Microphone Method (TMM) [13] and the Multipoint Method of Jones and Stiede [14]. Figure 5 is a diagram of the acquisition system while Figure 6 is a rendering of the NIT showing the pertinent features. Further details on the experimental setup can be found in Ref. 6.

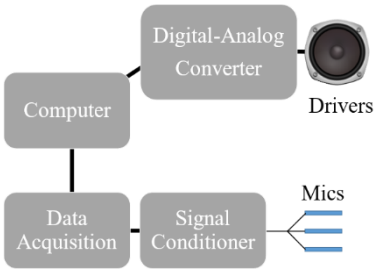

Figure 5. Normal Incidence Tube acquisition system diagram.

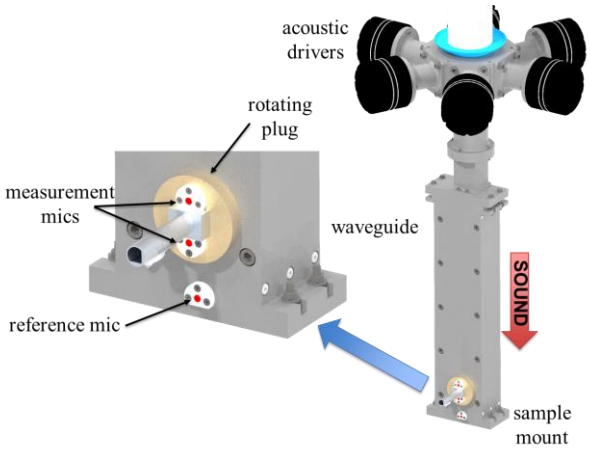

Figure 6. NASA Langley Normal Incidence Tube (NIT) general arrangement.

3.3.2 Grazing Flow Impedance Tube (Phase 2)

Grazing flow tests are performed on the liner samples using the GFIT. A schematic diagram of the setup is shown in Fig. 7. The GFIT is an acoustic wind tunnel with a 50.8 mm x 63.5 mm cross-section at the test section capable of centerline flow Mach numbers up to 0.6. Either of the two speaker arrays can be energized to achieve SPLs up to 150 dB depending on the desired orientation. For this investigation, the upstream array was employed to simulate conditions in the aft duct of a turbofan engine. An array of 95 pressure-field condenser microphones positioned along the length of the duct were used to measure the acoustic pressure profile. SPL and phase readings from each microphone were used to educe the liner acoustic impedance using the Straightforward Method of Watson and Jones [15].

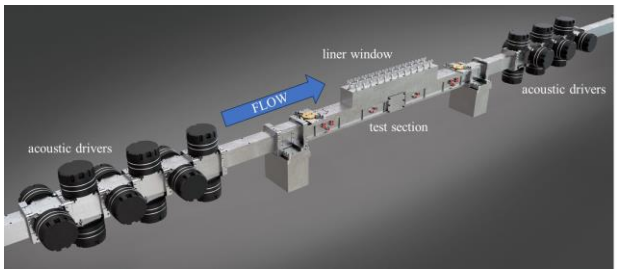

Figure 7. NASA Langley Grazing Flow Impedance Tube (GFIT) general arrangement.

3.3.3 Measurement Process

For both phases of testing, the Swept-Sine Method (SSM) [16] was used to obtain the complex acoustic cross spectra between the measurement microphones and the source signal supplied to the acoustic drivers. The acoustic source signal increases linearly in frequency from 400 to 3000 Hz during the measurement process and was amplitude modulated such that the total SPL at the sample surface was constant. A Vold-Kalman order tracking filter was employed to extract complex acoustic pressures at each microphone for the frequencies of interest. These pressures provided input for the various impedance eduction methods employed.
In the GFIT, grazing flow speed was set to duct centerline Mach numbers of 0.0, 0.3, and 0.5. At each Mach number, the acoustic source generates sine sweeps at SPLs of 120 dB and 140 dB for the same frequency range as used in the Phase 1 NIT testing.

4. RESULTS

4.1 Phase 1 - NIT

The impedance spectra for sample AM1S are shown in Figs. 8–9 at the two SPLs along with matching predictions. For both sound pressure levels, the model predicts the impedance behavior well with some deviation around antiresonance (~1800 Hz). Such deviations can be expected between model and experiment at 140 dB because the

model does not account for nonlinearities that create a reactance loss associated with perforates at high SPLs. There is work planned to incorporate a correction. Note that the frequency variation in both resistance and reactance decreases for the higher SPL which is a desired characteristic in a broadband absorber.

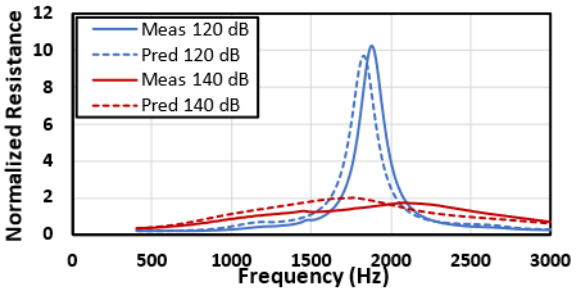

Figure 8. Comparison of measured AM1S acoustic resistance spectra to model predictions.

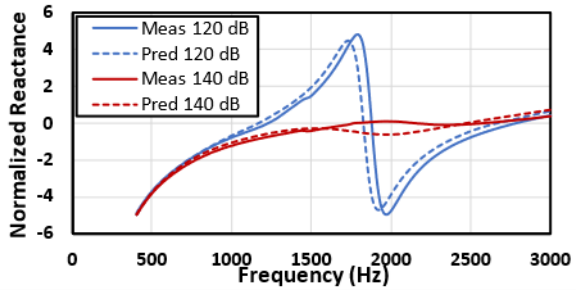

Figure 9. Comparison of measured AM1S acoustic reactance spectra to model predictions.

Figure 10 shows the computed and predicted absorption coefficient spectra for this configuration. As with impedance, the predictions are well matched to experimental results. Liners with normal incidence absorption coefficients above 0.4 have, historically, provided significant attenuation when evaluated in a grazing incidence environment such as the GFIT. Thus, one could expect reasonable broadband performance for this configuration above approximately 800 Hz and especially for higher sound pressure levels.

The addition of a second septum to the AM2S sample altered the characteristics of the impedance spectra as evident in Figs. 11–12. One can see in the 120 dB resistance spectra the appearance of a second antiresonance peak in the upper frequency range. The magnitudes of the peaks, however, are lessened compared to AM1S. Similar behavior is noted in the reactance, where the antiresonant spikes are not as sharp as AM1S.

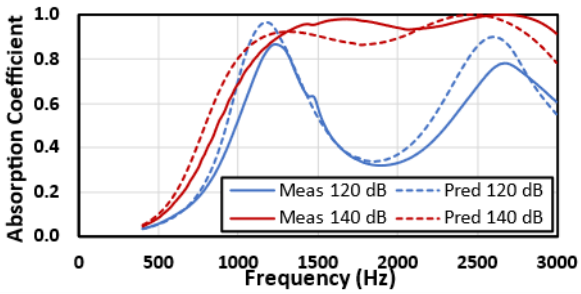

Figure 10. Comparison of measured AM1S absorption spectra to model predictions.

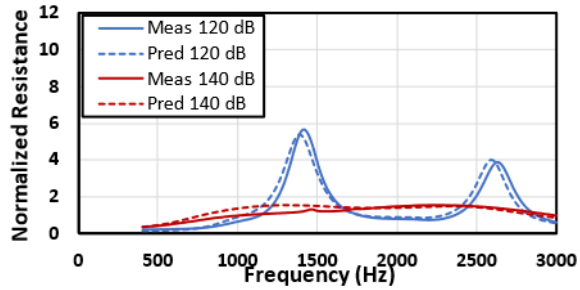

Figure 11. Comparison of measured AM2S acoustic resistance spectra to model predictions.

At 140 dB, there is little difference between the impedance spectra for both configurations. Interestingly, the agreement between experiment and modeling improved slightly for this configuration especially at the antiresonance frequencies. Enhanced absorption characteristics in the midfrequency range are observed for the 120 dB SPL case (Fig. 13), but performance at the design point of 140 dB was relatively unchanged compared to the simpler AM1S design.

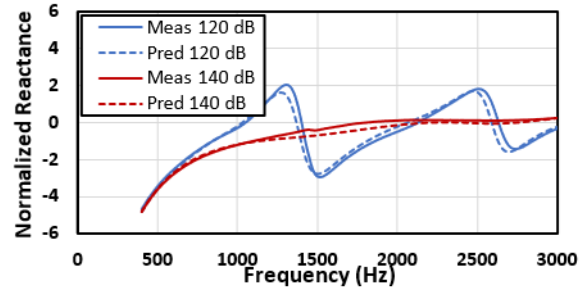

Figure 12. Comparison of measured AM2S acoustic reactance spectra to model predictions.

Based on these results, a decision was made to downselect the AM1S configuration for Phase 2 testing in the grazing flow environment of the GFIT. The addition of the second septum for AM2S does not appear to offer a significant acoustic benefit to justify the complexity and cost of production for flightworthy engine applications.

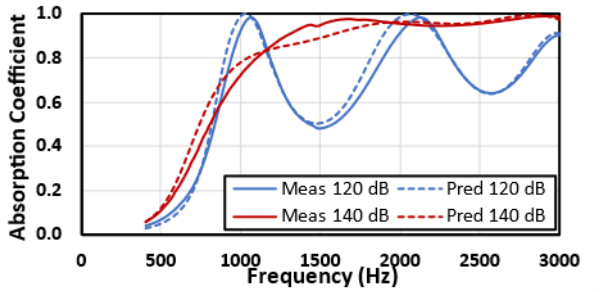

Figure 13. Comparison of measured AM2S absorption spectra to model predictions.

4.2 Phase 2 - GFIT

The intent of this investigation phase is to determine if the broadband absorption performance of the Simplified Septa concept observed in Phase 1 would carry over to a grazing flow environment. Ideally, one would see similar impedance characteristics for the design between the two test rigs, but it should be noted that the liner geometry was not optimized for the GFIT and grazing flow.

For the AM1S liner geometry, educed resistance and reactance spectra for an SPL of 120 dB are provided in Fig. 14 and 15, respectively, at the three test Mach numbers. At M=0.0, resistance and reactance are very similar to that seen in Phase 1 (Figs. 8–9) testing. Increasing flow speed shifts antiresonance to slightly higher frequencies with reduced peak values for both impedance quantities.

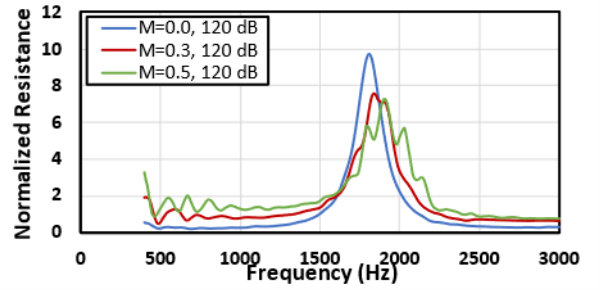

Figure 14. Educed AM1S acoustic resistance spectra for various flow Mach numbers, 120 dB SPL.

Resistance away from the peak increases as expected while reactance seems to flatten slightly for frequencies below antiresonance.

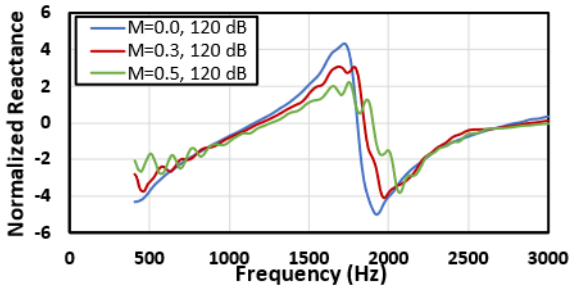

Figure 15. Educed AM1S acoustic reactance spectra for various flow Mach numbers, 120 dB SPL.

Increasing the acoustic excitation levels to 140 dB reduces the frequency variation in the impedance spectra for all Mach numbers, but variation is greater than observed in Phase 1 (Fig. 16–17). Resistance follows similar trends as the 120 dB data while reactance is only marginally affected by increasing the flow Mach number. The relative

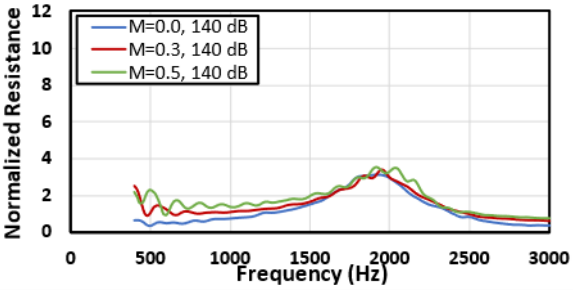

Figure 16. Educed AM1S acoustic resistance spectra for various flow Mach numbers, 140 dB SPL.

insensitivity to Mach number is somewhat expected given the POA of the facesheet as it is on the higher end of values used in engine liners. Such behavior could be desired in achieving predictable acoustic performance in practical applications.

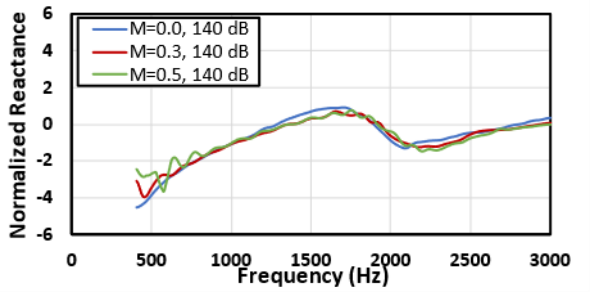

Figure 17. Educed AM1S acoustic reactance spectra for various flow Mach numbers, 140 dB SPL.

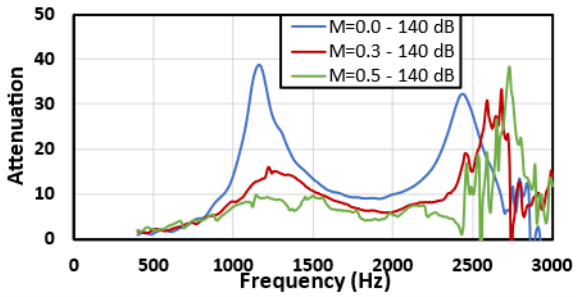

Figure 18. Calculated AM1S attenuation spectra for various flow Mach numbers, 140 dB SPL.

For both source SPLs, the educed impedance spectra exhibit an interesting characteristic with grazing flow. Some 'waviness' is observed in the impedance spectra, especially at lower frequencies and around antiresonance and becomes more pronounced at the higher Mach numbers. As the effect appears at both source levels, it is likely not acoustically induced but driven by some flow phenomenon. An initial hypothesis centers around possible compliance of the septum as its thickness (0.3 mm) is less than half of a typical facesheet. Further study is warranted to determine the cause, but the effect does not change the overall character of the spectra or the conclusions from this investigation.

Combining microphone SPL, relative phase and location data, one can compute the incident and reflected levels upstream and downstream of the liner sample. By subtracting pressure levels of the waves travelling with the flow, a simple measurement of liner attenuation can be computed. Data for both SPLs showed similar trends as the flow Mach number increased. As the higher source SPL is more relevant to most applications of this concept, only those results are presented. Figure 18 provides frequency spectra of this attenuation calculation for the AM1S sample at the three flow conditions for an SPL of 140 dB.

In keeping with the results from Phase 1 where the calculated absorption coefficient was above 0.4 for frequencies above 800 Hz, attenuation levels are generally greater than 5 dB up to the point the first higher-order mode is cut on (~2700 Hz @ M=0.0, ~2400 Hz @ M=0.5). Such levels have been shown previously to be sufficient for accurate impedance eduction [17]. The peaks in attenuation seen for the no-flow case are significantly reduced as Mach number increases. This is expected as the propagating wave has less time to interact with the liner due to flow convection.

Improved performance could be realized by altering the optimization objective function to target an impedance spectrum that produces greater attenuation in the GFIT. In developing SS liners for practical applications, this would be the likely approach.

5. CONCLUSIONS

Liner samples based on the Simplified Septa concept were constructed via AM and tested to determine their acoustic performance. Data from NIT were used to calculate impedance and absorption coefficient spectra for optimized single- and two-septa liners at two SPLs for frequencies between 400 and 3000 Hz. Comparisons of experimental results to predictions from a liner model based on ZKTL showed very good agreement. Both designs provided good absorption over a wide frequency range. The single-septa configuration was employed to create a larger liner for use in the GFIT to explore the effect of grazing flow. Acoustic data over the same frequency range, at 120 and 140 dB SPL and for Mach numbers up to 0.5 was used to educe impedance spectra and calculate the resulting attenuation levels. This phase of testing confirmed the introduction of grazing flow did not markedly alter the impedance characteristics of the liner. Thus, there is confidence the concept can be successfully employed in such noise control applications.

6. ACKNOWLEDGMENTS

The authors would like to thank Robert Andrews of the NASA Langley Additive Manufacturing Center for his efforts to construct the test samples. Appreciation also goes to NASA Langley Liner Physics Team members Christopher Shoemaker for processing the GFIT test data and Alonzo 'Max' Reid for acquiring the NIT data.

7. REFERENCES

[1] Van Zante, D, Nark, D. M., Fernandez, H., "Propulsion Noise Reduction Research in the NASA Advanced Air Transport Technology Project," *International Society for Air Breathing Engines 2017*, Manchester, UK, Sept 2017.

[2] "The NASA Acoustically Treated Nacelle Program," *Proc. of the Aircraft Noise Symp.* (Acoustical Duct Treatments for Aircraft), Invited Tutorial Papers presented at the *77th Meeting of the Acoustical Society of America*, Philadelphia, PA, Apr. 1969.

[3] "Study and Development of Turbofan Nacelle Modifications to Minimize Fan-Compressor Noise Radiation," Vol. IV – Flight-worthy Nacelle Development, Prepared by The Boeing Company, NASA CR-1714, Jan. 1971.

[4] Nark, D. M. and Jones, M. G., "Design of an Advanced Inlet Liner for the Quiet Technology Demonstrator 3," AIAA 2019-2764, *25th AIAA/CEAS Aeroacoustics Conference*, Delft, The Netherlands, May 2019.

[5] Bielak, G. W., Premo, J. W., and Hersh, A. S., "Advanced Turbofan Duct Liner Concepts," NASA CR-1999-209002, February 1999.

[6] Howerton, B. M., Kreitzman, J., and Solano, C., "Extending Acoustic Liner Bandwidth with Simple Embedded Septa," AIAA 2024-3302, *30th AIAA/CEAS Aeroacoustics Conference*, Rome, Italy, June 2024.

[7] Zwikker, C., and Kosten, C., *Sound Absorbing Materials*, Elsevier, Amsterdam, 1949.

[8] Tijdeman, H., "On the propagation of sound waves in cylindrical tubes," *Journal of Sound and Vibration*, Vol. 39, No. 1, pp. 1–33, March 1975.

[9] Parrott, T., and Jones, M., "Parallel-element liner impedances for improved absorption of broadband sound in ducts," *Noise Control Engineering Journal*, Vol. 43, No. 6, pp. 183–195, 1995.

[10] Kreitzman, J., and Jones, M., "Toward Fully 3D-Printed Two Degree of Freedom Acoustic Liners," AIAA Paper 2024-2801, *AIAA SCITECH 2024*, Orlando, FL, Jan 2024.

[11] Johnson, S., "The NLopt nonlinear-optimization package," 2021. http://github.com/stevengj/nlopt.

[12] Powell, M., "The BOBYQA algorithm for bound constrained optimization without derivatives," *Department of Applied Mathematics and Theoretical Physics, Cambridge England, technical report NA2009/06*, 2009.

[13] J. Chung and D. Blaser, "Transfer function method of measuring in-duct acoustic properties: I. theory," *Journal of the Acoustical Society of America*, vol. 68, pp. 907–921, 1980.

[14] Jones, M. G., and Stiede, P. E., "Comparison of Methods for Determining Specific Acoustic Impedance," *Journal of the Acoustical Socicy of America*, Vol. 101, No. 5, Pt. 1, pp. 2694-2704, May 1997.

[15] Watson, W. R., and Jones, M. G., "A comparative study of four impedance eduction methodologies using several test liners," AIAA 2013-2274, *19th AIAA/CEAS Aeroacoustics Conference*, Berlin, DE, May 2013.

[16] Howerton, B. M., Vold, H, and Jones, M. G., "Application of Swept-Sine Excitation for Acoustic Impedance Eduction," AIAA 2019-2487, *25th AIAA/CEAS Aeroacoustics Conference*, Delft, NE, May 2019.

[17] Jones, M. G., Nark, D. M., and Howerton B. M., "Impedance eduction for uniform and multizone acoustic liners". *International Journal of Aeroacoustics*, Vol. 20, Nos. 5-7, pp. 458-477, Sept. 2021.